Eur. Phys. J. D **8**, 101–110 (2000)

THE EUROPEAN PHYSICAL JOURNAL D

EDP Sciences
© Società Italiana di Fisica
Springer-Verlag 2000

Quantum theory of fluctuations in a cold damped accelerometer

F. Grassia[1,a], J.-M. Courty[1,b], S. Reynaud[1,c], and P. Touboul[2,d]

[1] Laboratoire Kastler Brossel[e], UPMC case 74, 4 place Jussieu, 75252 Paris Cedex 05, France
[2] Département de Mesures Physiques, ONERA, 29 avenue de la division Leclerc, B.P. 72, 92322 Chatillon Cedex, France

Received 20 April 1999 and Received in final form 2 July 1999

Abstract. We present a quantum network approach to real high sensitivity measurements. Thermal and quantum fluctuations due to active as well as passive elements are taken into account. The method is applied to the analysis of the capacitive accelerometer using the cold damping technique, developed for fundamental physics in space by ONERA and the ultimate limits of this instrument are discussed. It is confirmed in this quantum analysis that the cold damping technique allows one to control efficiently the test mass motion without degrading the noise level.

PACS. 42.50.Lc Quantum fluctuations, quantum noise, and quantum jumps – 04.80.Cc Experimental tests of gravitational theories – 07.50.-e Electrical and electronic components, instruments, and techniques

1 Introduction

When discussing ultimate limits in ultrasensitive measurements, we have to take into account fundamental fluctuation processes as well as a realistic description of the measurement device. This requires to treat in the same theoretical framework a number of problems which are often tackled by different approaches. Real measurements always have a finite time resolution, that is also a characteristic frequency bandwidth, as well as a finite duration. The measurement is never infinitely precise and fluctuations are superimposed to the signal. Ultrasensitive measurement devices often make use of active systems either for amplifying the signal to a readable level or to make the system work around its optimal operating point with the help of feedback loops. Feedback loops can also be used to modify the natural frequency response and, in particular, to perform an optimal damping of moving elements.

The aim of the present paper is to develop an approach of ultrasensitive measurements taking into account these various problems. In particular, we want to treat thermal as well as quantum fluctuations for systems containing active as well as dissipative elements. The approach will be illustrated by analyzing the sensitivity of a cold damped capacitive accelerometer developed for fundamental physics applications in space [1–3]. In this measurement system, feedback loops are used to keep the proof mass perfectly centered in the accelerometer cage and to damp its motion without adding the thermal fluctuations which would necessarily accompany a passive damping. With this technique, fluctuations are reduced to an effective temperature well below the operating temperature [4]. The cold damping technique is known to be compatible with very high sensitivities of the measurement [5]. However the question of ultimate sensitivities compatible with the existence of quantum fluctuations remains open. This question is important not only for a better understanding of the instrument but also for the long term purpose of an improvement of its performances. For earth based detection of gravitational waves, highly effective motion isolation and feedback controlled noise reduction is developed [6,7]. The cryogenic accelerometers planned for future space mission such as LISA will require very low noise levels and they use cryogenic techniques.

Relations between fluctuations and dissipation have been first discovered by Einstein which studied the viscous damping of mechanical systems [8]. Another important application was the study of Johnson-Nyquist noise in resistive electrical elements [9]. These general thermodynamical relations were widely studied in the framework of linear response theory [10,11]. In the limit of a null temperature, they reproduce quantum fluctuations required by Heisenberg inequalities [12]. Important progress have been made during the last two decades towards a better control of the effect of quantum fluctuations on ultrasensitive measurements [13,14]. It has been shown that it was possible to bypass the limitations usually associated with quantum noise by using back action evading measurements or quantum non demolition techniques [15–18]. Fluctuations associated with amplification were also extensively studied [19–21]; they determine the ultimate

[a] e-mail: grassia@spectro.jussieu.fr
[b] e-mail: courty@spectro.jussieu.fr
[c] e-mail: reynaud@spectro.jussieu.fr
[d] e-mail: touboul@onera.fr
[e] Laboratoire de l'Université Pierre et Marie Curie, de l'École Normale Supérieure et du Centre National de la Recherche Scientifique.

performance of linear amplifiers [22,23] and they may be used to reduce inloop quantum fluctuations with feedback [24,25].

In the present paper we will study this kind of measurement systems by using a systematic approach which may be termed as "quantum network theory". Initially designed as a quantum extension of the classical theory of electrical networks [26], this theory was mainly developed through applications to optical systems [27,28]. It can be viewed as a generalization of the linear response theory [29] and is also fruitful for analysing non-ideal quantum measurements with active elements [30] as soon as a quantum theory of ideal operational amplifier is available [31]. The main features of this approach are recalled in Section 2.

Here, this theory will be illustrated by a study of an electromechanical measurement system comprising active and dissipative components coupled to a capacitive position sensor. The parametric nature of the electromechanical coupling allows the use of a frequency transfer technique in order to eliminate the influence of the $1/f$ noise in the electric part of the device. Active elements are used for preamplifying the position sensing signal to a readable level as well as for controlling the mechanical motion through a feedback loop. The main features of the cold damped capacitive accelerometer are described in Section 3. Then the capacitive sensor is analysed in absence of servo control in Section 4 and in presence of servo control in Section 5. These results are used in Section 6 to evaluate the ultimate sensitivity of the measurement system, which is found to be essentially determined by the free mechanical impedance of the proof mass and the ratio of the frequencies involved in the frequency transfer performed by the transducer.

2 Noise in electromechanical systems

In this section we present the basic elements of the quantum network approach. Quantum and thermal fluctuations in dissipative and active systems are all described in terms of quantum fields. All the descriptions are given in the frequency domain and the convention of quantum mechanics is used for the Fourier transform. The electronics convention may be recovered by substituting j to $-i$.

In a quantum network approach, the various fluctuations entering the system, either by dissipative or by active elements, are described by input fields in noise lines coupled to a reactive network (see Fig. 1).

In particular, a resistance R_p is modeled as a semi-infinite coaxial line p with characteristic impedance R_p. The voltage U_p and current I_p associated with the resistance are the inward and outward fields p^{in} and p^{out} evaluated at the end of this line

$$I_p = \sqrt{\frac{\hbar\,|\omega|}{2R_p}}\left(p^{\text{out}} - p^{\text{in}}\right),$$
$$U_p = \sqrt{\frac{\hbar\,|\omega|\,R_p}{2}}\left(p^{\text{out}} + p^{\text{in}}\right). \qquad (1)$$

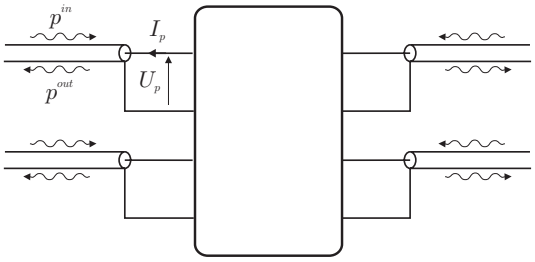

Fig. 1. Representation of an electrical circuit as a quantum network. The central box is a reactive multipole which connects noise lines corresponding to the fluctuations entering the system, either by dissipative or by active elements. For example, the upper left port p with voltage U_p and current I_p is connected to a line of impedance R_p with inward and outward fields p^{in} and p^{out}.

These equations may be written equivalently

$$U_p = R_p I_p + \sqrt{2\hbar\,|\omega|\,R_p}\,p^{\text{in}},$$
$$p^{\text{out}} = \sqrt{\frac{2}{\hbar\,|\omega|\,R_p}}\,U_p - p^{\text{in}}. \qquad (2)$$

The first equation in (2) is the standard current-voltage relation for a resistance with the Johnson-Nyquist noise described as the input fields p^{in} going to the end of the line. The second equation gives the output fields p^{out} emitted back to the line. In the following, these fields are used either to feed other elements of the system or to perform a measurement by extracting information from the system of interest through a line considered as the detection channel.

Input fields p^{in} are described as free fields in a two-dimensional quantum field theory. They obey the standard commutation relation of such a theory

$$\left[p^{\text{in}}\left[\omega\right], p^{\text{in}}\left[\omega'\right]\right] = 2\pi\delta\left(\omega+\omega'\right)\varepsilon\left(\omega\right) \qquad (3)$$

where $\varepsilon(\omega)$ denotes the sign of the frequency ω. This relation just means that the positive and negative frequency components correspond respectively to the annihilation and creation operators of quantum field theory. Input fields corresponding to different lines commute with each other. For simplicity, the fields incoming through the various ports are supposed to be uncorrelated with each other. The interaction with non linear reactive elements are linearized around the working point of the system. With the whole network is then associated a scattering S matrix, also called repartition matrix, describing the transformation from the input fields to the output ones. The output fields p^{out} are also free fields which obey the same commutation relations (3) as the input ones. Hence, the S matrix must be unitary in order to preserve the field commutation relations.

Input fluctuations are characterized by a noise spectrum σ^{in}_{pp} with its well-known expression for a thermal

equilibrium at a temperature T_p

$$\left\langle p^{\rm in}\left[\omega\right]\cdot p^{\rm in}\left[\omega'\right]\right\rangle = 2\pi\delta\left(\omega+\omega'\right)\sigma_{pp}^{\rm in}\left[\omega\right],$$
$$\sigma_{pp}^{\rm in}\left[\omega\right] = \frac{1}{2}\coth\frac{\hbar\left|\omega\right|}{2k_{\rm B}T_p}\cdot \tag{4}$$

The symbol "$\cdot$" denotes a symmetrized product for quantum operators and $k_{\rm B}$ is the Boltzmann constant. The energy per mode will be denoted in the following as an effective temperature

$$k_{\rm B}\Theta_p = \hbar\left|\omega\right|\sigma_{pp}^{\rm in} = \frac{\hbar\left|\omega\right|}{2}\coth\frac{\hbar\left|\omega\right|}{2k_{\rm B}T_p}\cdot \tag{5}$$

This effective temperature $k_{\rm B}\Theta_p$ reproduces the zero point energy $\hbar\left|\omega\right|/2$ at the limit of zero temperature and the classical result $k_{\rm B}T_p$ at the high temperature limit. The output fields are also characterized by noise spectra $\sigma_{pp}^{\rm out}$ which are different from those associated with input fields, due to the interaction with the system. In fact the analysis of the measurement sensitivity essentially consists in an evaluation of these functions.

In the capacitive sensor used in the accelerometer, a frequency transposition technique is used to reduce the $1/f$ electrical noise. The mechanical signal at frequency Ω is imprinted on the sidebands $\omega_{\rm t}\pm\Omega$ of an electrical carrier oscillating at frequency $\omega_{\rm t}$. Such a signal is described by quadrature components

$$p_1\left[\Omega\right] = p\left[\omega_{\rm t}+\Omega\right]+p\left[-\omega_{\rm t}+\Omega\right],$$
$$p_2\left[\Omega\right] = \frac{p\left[\omega_{\rm t}+\Omega\right]+p\left[-\omega_{\rm t}+\Omega\right]}{\rm i}\cdot \tag{6}$$

Assuming that $\omega_{\rm t}\gg\Omega$, the noise spectra of these quadratures is given by

$$\sigma_{p_1p_1}^{\rm in} = \sigma_{p_2p_2}^{\rm in} = \frac{2k_{\rm B}\Theta_p}{\hbar\omega_{\rm t}} \tag{7}$$

where Θ_p is evaluated from (5) for a frequency equal to $\omega_{\rm t}$.

The previous discussion of electrical elements is easily extended to include mechanical elements. A mass damped by a viscous force is described by equations similar to (1)

$$V_{\rm m} = \sqrt{\frac{\hbar\left|\Omega\right|}{2H_{\rm m}}}\left(m^{\rm out}-m^{\rm in}\right),$$
$$F_{\rm m} = \sqrt{\frac{\hbar\left|\Omega\right|H_{\rm m}}{2}}\left(m^{\rm out}+m^{\rm in}\right), \tag{8}$$

or equivalently

$$F_{\rm m} = H_{\rm m}V+\sqrt{2\hbar\left|\Omega\right|H_{\rm m}}m^{\rm in},$$
$$m^{\rm out} = \sqrt{\frac{2}{\hbar\left|\Omega\right|H_{\rm m}}}F_{\rm m}-m^{\rm in}. \tag{9}$$

In these equations, $H_{\rm m}$ is the friction coefficient, $V_{\rm m}$ the velocity of the mass, $F_{\rm m}$ the force acting on the mass, Ω the mechanical frequency and $m^{\rm in}$ and $m^{\rm out}$ are input and output quantum fields in an equivalent mechanical line m. In particular, the fluctuating Langevin force is proportional to the input fluctuations $m^{\rm in}$. The free fields $m^{\rm in}$ and $m^{\rm out}$ obey the same commutation relation (3) as for electrical lines and an effective temperature is defined as in (5)

$$k_{\rm B}\Theta_{\rm m} = \hbar\left|\Omega\right|\sigma_{\rm mm}^{\rm in} = \frac{\hbar\left|\Omega\right|}{2}\coth\frac{\hbar\left|\Omega\right|}{2k_{\rm B}T_{\rm m}}\cdot \tag{10}$$

The description of fluctuations in active elements requires further developments. In the present paper, attention is restricted to active elements built on ideal operational amplifiers working in the limits of an infinite input impedance, a null output impedance and an infinite gain. Such an amplifier is described as a quantum network connected to the left (input) port, the right (output) port and two lines needed to describe these noise generators associated with the amplifier [31].

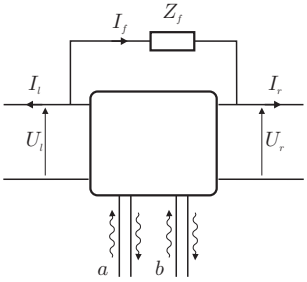

Fig. 2. Representation of the ideal operational amplifier as a quantum network with a left (input) port l and a right (output) port r. The input and output impedances are respectively infinite and null. The amplifier works in the limit of infinite gain with a reactive feedback $Z_{\rm f}$. The voltage and current noises of the amplifier are modeled as input fields in the two noise lines a and b.

The equations of the amplifier, schematized in Figure 2, are read as

$$U_{\rm l}\left[\omega\right] = U_{\rm r}\left[\omega\right]+Z_{\rm f}I_{\rm f}\left[\omega\right]$$
$$= \sqrt{2\hbar\left|\omega\right|R_{\rm a}}\left(a^{\rm in}\left[\omega\right]-b^{\rm in}\left[-\omega\right]\right),$$
$$I_{\rm l}\left[\omega\right]+I_{\rm f}\left[\omega\right] = \sqrt{\frac{2\hbar\left|\omega\right|}{R_{\rm a}}}\left(a^{\rm in}\left[\omega\right]+b^{\rm in}\left[-\omega\right]\right). \tag{11}$$

$U_{\rm l}$ and $U_{\rm r}$ are the voltages at the left and right ports, $I_{\rm l}$ the current at the left port, $I_{\rm f}$ the current across the reactive impedance $Z_{\rm f}$ (Re$Z_{\rm f}=0$) used to adjust the transimpedance gain of the amplifier. The voltage noise and current noise associated with the amplification are described by two fields $a^{\rm in}$ and $b^{\rm in}$ which verify the free field commutation relation (3). The field $b^{\rm in}$ appears in the equation after a conjugation which interchanges annihilation and creation operators. The presence of such a conjugation, already known for linear amplifiers [22,23], plays an important role when commutators are evaluated. It can be forgotten when symmetrized correlation functions are computed and will be considered as implicit in forthcoming equations. In (11), the impedance $R_{\rm a}$,

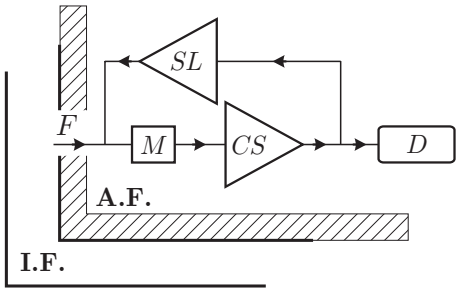

Fig. 3. The accelerometer is designed to detect the motion of the frame **A.F.** defined by the accelerometer cage with respect to an inertial frame **I.F**. Any acceleration, seen as an inertial force F acting on the proof mass M, is detected by a capacitive sensor CS. The signal of this sensor is used for the force detection D as well as for keeping the mass centered with respect to the cage through a servo-control loop SL.

which characterizes the amplifier noise, is derived from the ratio of the voltage and current noises

$$R_{\mathrm{a}} = \sqrt{\frac{\sigma_{\mathrm{UU}}}{\sigma_{\mathrm{II}}}}\,. \tag{12}$$

These fluctuations have been assumed to be phase-insensitive, *i.e.* to be the same for any field quadrature. Although these assumptions are not mandatory for the forthcoming analysis, the impedance R_{a} is considered as constant over the spectral domain of interest and the effective temperature Θ_{b} is taken equal to Θ_{a}.

3 General description of the accelerometer

The capacitive accelerometer operation is presented in Figure 3.

The instrument is designed to detect the acceleration of the accelerometer cage due to any external force. To this aim the relative motion of the proof mass M with respect to the frame defined by the cage is measured by the capacitive sensor. An important characteristics of the mass is its free mechanical impedance determined by a restoring force to the center of the cage with a stiffness K and a viscous damping with a coefficient H_{m}. Depending on the physical origin of these effects, K and H_{m} may be frequency dependent.

Dedicated to space applications, the accelerometer operation is based on the electrostatic suspension of the proof mass in all spatial directions. Hence, the mass is kept centered with respect to its cage through 3 servo-control loops demanded at least for stability (Earnshaw theorem). The acceleration signal is in fact extracted from the knowledge of the electrostatic force necessary to maintain the mass centered. In the real device, the control of position and attitude is performed by six servo-control channels acting separately. For simplicity, only one of the channels, corresponding to a translation degree of freedom, is analyzed in this paper.

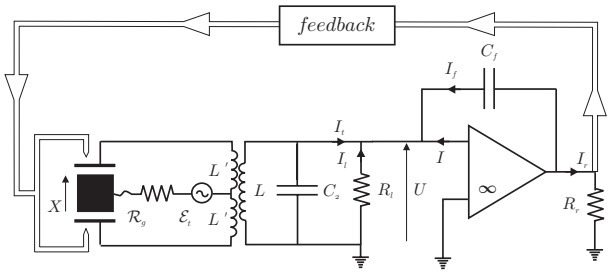

Fig. 4. Scheme of the capacitive sensor. The proof mass is placed between two electrodes. The position dependent capacitances are polarized by an AC sinewave source which induces a mean current at frequency ω_{t} in the symmetrical mode. The mass displacement is read as the current induced in the antisymmetric mode. An additional capacitance C_2 is inserted to make the antisymmetric mode resonant with ω_{t}. The electrical losses due to the quality factor of the transformer are modeled as a resistance R_{l} for the antisymmetric mode. The signal is detected after an ideal operational amplifier with capacitive feedback C_{f} followed by a synchronous demodulation (not represented on this picture). The impedance of the detection line plays the role of a further resistance R_{r}. The detected signal then feds the servo loop used to keep the mass centered with respect to the cage.

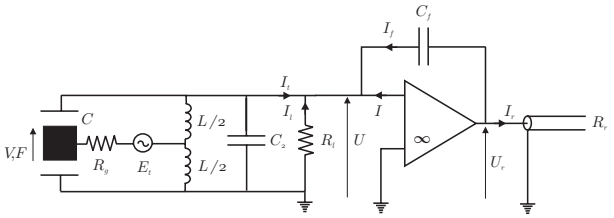

Fig. 5. Equivalent scheme of the capacitive sensor. The transformer of Figure 4 is replaced by the two inductances $L/2$ while the associated losses are modeled as a resistance R_{l}. The other impedances are modified accordingly.

As depicted in Figure 4, the proof mass is placed between two symmetric electrodes supported by the instrument cage which create two position dependent capacitances. When the mass is centered in its cage, both capacities are equal and the capacitance bridge is balanced. A displacement of the mass creates an asymmetry of the bridge detected thanks to a differential transformer and a pumping signal applied on the mass. Conversely, voltages applied on these electrodes allow to exert electrostatic forces on the mass. Capacitances are thus used for position sensing as well as for generating the suspension force. Coupling between the primary and secondary coils of the transformer being assumed ideal, the transformer can be replaced by the equivalent circuit presented in Figure 5. It is considered from now on that this transformation has been performed and the circuit impedances redefined accordingly.

The capacitances are polarized by an AC source of frequency ω_{t} which is chosen large enough for avoiding electrical $1/f$ noise and for using low noise electronics. The sinewave source E_{t} induces current at frequency ω_{t} in the transformer symmetrical mode. In this static

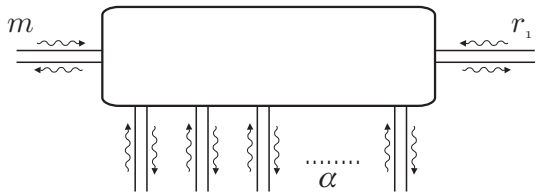

Fig. 6. Description of the accelerometer as a quantum network performing input output transformations on a number of lines. m is the mechanical line describing mechanical fluctuations as well as the measured signal, that is the external force $F_{\rm ext}$. r_1 is the detection line. α labels the other lines $a_1, a_2, b_1, b_2, r_1, r_2, l_1, l_2$ which contribute to noise.

and symmetric configuration, the current in the antisymmetric mode is zero and the fluctuations of the two modes are uncoupled. Then a motion of the proof mass at frequency Ω induces an asymmetry in the system and creates sidebands on this electrical carrier $\omega_{\rm t}$. The effect of this asymmetry will be treated in a linear approximation with respect to the deviations from the steady state equilibrium. The current induced in the antisymmetric mode is thus proportional to the current in the symmetrical mode and to the mass displacement. With this approximation, the fluctuations of the symmetrical mode remain uncoupled to the antisymmetric mode and to the mass motion. This is why the symmetric mode will be disregarded in the following. In order to optimize the signal to noise ratio, an additional capacitance C_2 is inserted which makes the antisymmetric mode resonant with $\omega_{\rm t}$. The electrical losses are mainly due to the quality factor of the transformer and they are modeled by a resistance $R_{\rm l}$ for the antisymmetric mode.

The signal imprinted on the antisymmetric mode is detected after an ideal operational amplifier with capacitive feedback (charge amplifier) followed by a synchronous demodulation. This provides a low frequency voltage proportional to the displacement of the mass. In a quantum network approach, the signal is delivered by the capacitive sensor as the output field of a detection line the impedance of which plays the role of a further resistance $R_{\rm r}$. The description of the sensor is given in more detail in the next section. This signal is used to feed the servo loop and keep the mass at its equilibrium. Through the mass motion, it contains information on the external forces acting on the mass. The noise added by the measurement device to the measured observable is evaluated in the next sections, by considering input fluctuations coming from all noise lines in the quantum network model of Figure 6.

It is in fact impossible to reach a stable equilibrium with a passive electrostatic configuration. This is why the mass is actively maintained at its equilibrium position by the generated electrostatic forces tailored through the servo-control loop. The feedback control includes a proportional and a derivation term. The generated electrostatic force proportional to the measured mass displacement defines the servo-loop stiffness and, more or less, the measurement bandwidth of the accelerometer. The force proportional to the mass velocity introduces a motion damping to the benefit of the control loop stability. This technique of active friction is equivalent to an effective damping with reduced fluctuations in comparison to those necessarily associated with a passive mechanical damping. This is why it is called a cold damping technique. It will turn out that the added fluctuations may even be smaller than the fluctuations associated with the residual mechanical friction although the latter is much less efficient than the active friction.

4 The capacitive sensor

In this section the capacitive sensor is analyzed in the absence of servo control loop, with the equivalent electrical circuit of Figure 5.

For a mass motion to be detected at frequency Ω, the signal is transposed by the electromechanical transducer to sidebands $\omega = \pm\omega_{\rm t} + \Omega$ of the carrier frequency $\omega_{\rm t}$. The electrical quadratures are defined as in equations (6) and they are dealt with separately so that the transducer appears as a three port network. The first port is a mechanical one and corresponds to the velocity $V_{\rm fr}$ of the free running proof mass and the force F exerted on it. The two other ports are electrical ones with the voltages $U_{{\rm t},n}$ and currents $I_{{\rm t},n}$ of the two quadratures $n = 1, 2$. The three port network is described by an electromechanical impedance matrix

$$\begin{aligned} F &= \left(\frac{{\rm i}K}{\Omega} - {\rm i}M\Omega\right) V_{\rm fr} + \varkappa_{\rm t} Z_{\rm t} I_{\rm t1}, \\ U_{\rm t1} &= Z_{\rm t} I_{\rm t1}, \\ U_{\rm t2} &= 2{\rm i}\varkappa_{\rm t} Z_{\rm t} \frac{\omega_{\rm t}}{\Omega} V_{\rm fr} + Z_{\rm t} I_{\rm t2}, \\ Z_{\rm t} &= -\frac{1}{2{\rm i}\Omega C_{\rm t}}\cdot \end{aligned} \tag{13}$$

${\rm i}K/\Omega - {\rm i}M\Omega$ is the reactive part of the mechanical impedance of the proof mass expressed in terms of mass M and stiffness K. $Z_{\rm t}$ is the electrical impedance evaluated at both frequencies $\pm\omega_{\rm t} + \Omega$ for a resonant circuit tuned at the polarization frequency $\omega_{\rm t}$. $\varkappa_{\rm t}$ is an electromechanical coupling constant proportional to the amplitude of the field created by the sinewave electrical source applied to the mass. This impedance matrix shows that the mechanical motion can be detected through the electrical quadrature 2 whereas it is unaffected by the fluctuations coming through this port. Meanwhile the mechanical motion is affected by the input fluctuations of the electrical quadrature 1. These features, typical of a quantum non demolition coupling between electrical and mechanical elements, is discussed in more detail in [30].

Fluctuations associated with losses are taken into account as the input fields $l^{\rm in}$ coming to the transducer through the electrical line of impedance $R_{\rm l}$ as in equation (2) and as the input fields $m^{\rm in}$ coming through the mechanical line of impedance $H_{\rm m}$ as in equation (8). The external force $F_{\rm ext}$ to be detected comes as a mean field superimposed to the fluctuations $m^{\rm in}$ so that the

equation of motion of the free running mass may be written

$$\Xi_{\rm m} V_{\rm fr} = F_{\rm ext} - \varkappa_{\rm t} Z_{\rm t} I_{\rm t1} - \sqrt{2\hbar\,|\Omega|\,H_{\rm m}}\, m^{\rm in}$$
$$\Xi_{\rm m} = H_{\rm m} - {\rm i}M\Omega + \frac{{\rm i}K}{\Omega} \tag{14}$$

$\Xi_{\rm m}$ is the full mechanical impedance of the proof mass in its free running regime, now including not only the reactive part but also the damping coefficient $H_{\rm m}$.

The voltage and currents fluctuations associated with the amplifier have then to be considered. In the configuration studied here, equations (11) are replaced by

$$U_{\rm l}\,[\omega] = U_{\rm t}\,[\omega] = U_{\rm r}\,[\omega] + Z_{\rm f} I_{\rm f}\,[\omega]$$
$$= \sqrt{2\hbar\,|\omega|\,R_{\rm a}}\left(a^{\rm in}\,[\omega] - b^{\rm in}\,[-\omega]\right)$$
$$I_{\rm l}\,[\omega] + I_{\rm f}\,[\omega] + I_{\rm t}\,[\omega] = \sqrt{\frac{2\hbar\,|\omega|}{R_{\rm a}}}\left(a^{\rm in}\,[\omega] + b^{\rm in}\,[-\omega]\right)$$
$$Z_{\rm f} = \frac{1}{-{\rm i}\omega_{\rm t} C_{\rm f}} \tag{15}$$

with $C_{\rm f}$ the capacitor in the feedback loop of the amplifier. To complete the set of equations associated with the electromechanical transducer, the detected signal is the output field $r^{\rm out}$ which comes out from the line r of impedance $R_{\rm r}$ and is therefore related to the voltage $U_{\rm r}$ as in equation (2).

Equations (13–15) may be solved to obtain the output field as well as the mass velocity. The latter quantity is expressed in terms of the input fields (α labels the input noise lines $m, a_1, a_2, b_1, b_2, r_1, r_2, l_1, l_2$; see Fig. 6)

$$\Xi_{\rm m} V_{\rm fr} = F_{\rm ext} + \sum_\alpha \lambda_\alpha \alpha^{\rm in},$$
$$\lambda_{\rm m} = -\sqrt{2\hbar\,|\Omega|\,H_{\rm m}},$$
$$\lambda_{\rm a_1} = -\lambda_{\rm b_1} = -\sqrt{2\hbar\omega_{\rm t} R_{\rm a}}\,\varkappa_{\rm t},$$
$$\lambda_{\rm a_2} = \lambda_{\rm b_2} = \lambda_{\rm r_1} = \lambda_{\rm r_2} = \lambda_{\rm l_1} = \lambda_{\rm l_2} = 0. \tag{16}$$

The velocity of the proof mass coupled to the electromechanical transducer thus appears as a linear combination of the external force $F_{\rm ext}$ to be measured and of input fields in the noise lines associated either with dissipative elements or with active ones. A number of coefficients λ_α are null as a consequence of our simplifying assumptions, in particular the assumption of the ideal operational amplifier. There remain only two contributions to be discussed. The first corresponds to the Langevin force fluctuations associated to the mechanical damping and proportional to fields $m^{\rm in}$. The second one comes from the voltage noise at the input of the amplifier which is transformed to a back action force exerted on the mass by the capacitive transducer. Accordingly, the noise spectrum characterizing the velocity fluctuations is the sum of two contributions which depend on the effective temperatures $\Theta_{\rm m}$ and $\Theta_{\rm a}$ associated respectively with the mechanical and the amplification noise through (10) and (5)

$$|\Xi_{\rm m}|^2\,\sigma_{V_{\rm fr}V_{\rm fr}} = \sum_\alpha |\lambda_\alpha|^2\,\sigma^{\rm in}_{\alpha\alpha}$$
$$= 2H_{\rm m} k_{\rm B}\Theta_{\rm m} + 8R_{\rm a}\varkappa_{\rm t}^2 k_{\rm B}\Theta_{\rm a}. \tag{17}$$

The output signal $r_1^{\rm out}$ is then evaluated by solving the same equations (13–15). As the velocity, it is a linear combination of the external force $F_{\rm ext}$ and of input fields in the various noise lines. When the expression of $r_1^{\rm out}$ is normalized so that the coefficient of proportionality appearing in front of $F_{\rm ext}$ is reduced to unity, the force estimator $\widehat{F}_{\rm ext}$ is just the sum of this external force to be measured and of the equivalent input force noise

$$\widehat{F}_{\rm ext} = \sqrt{\frac{\hbar R_{\rm r}}{2\omega_{\rm t}}}\,\frac{\Omega\Xi_{\rm m}}{2\varkappa_{\rm t} Z_{\rm f}}\, r_1^{\rm out}$$
$$= F_{\rm ext} + \sum_\alpha \mu_\alpha \alpha^{\rm in}. \tag{18}$$

The coefficients μ_α are found to be

$$\mu_{\rm m} = -\sqrt{2\hbar\,|\Omega|\,H_{\rm m}},$$
$$\mu_{\rm l_2} = -\frac{{\rm i}\Omega\sqrt{\hbar}}{\sqrt{2R_{\rm l}\omega_{\rm t}}\varkappa_{\rm t}}\Xi_{\rm m}, \quad \mu_{l_1} = 0,$$
$$\mu_{\rm r_1} = -\frac{\Omega\sqrt{\hbar R_{\rm r}}}{2\sqrt{2\omega_{\rm t}} Z_{\rm f}\varkappa_{\rm t}}\Xi_{\rm m}, \quad \mu_{\rm r_2} = 0,$$
$$\mu_{\rm a_1} = -\mu_{\rm b_1} = \sqrt{2\hbar R_{\rm a}\omega_{\rm t}}\left(-\varkappa_{\rm t} + \frac{\Omega}{2\varkappa_{\rm t}\omega_{\rm t} Z_{\rm f}}\Xi_{\rm m}\right),$$
$$\mu_{\rm a_2} = -\frac{{\rm i}\Omega\sqrt{\hbar R_{\rm a}}}{\sqrt{2}\varkappa_{\rm t}\sqrt{\omega_{\rm t}}}\Xi_{\rm m}\left(\frac{1}{R_{\rm a}} - \frac{1}{R_{\rm l}} - \frac{1}{Z_{\rm t}}\right),$$
$$\mu_{\rm b_2} = -\frac{{\rm i}\Omega\sqrt{\hbar R_{\rm a}}}{\sqrt{2}\varkappa_{\rm t}\sqrt{\omega_{\rm t}}}\Xi_{\rm m}\left(\frac{1}{R_{\rm a}} + \frac{1}{R_{\rm l}} + \frac{1}{Z_{\rm t}}\right). \tag{19}$$

The comparison of equations (16, 19) shows that all the terms λ_α of the expression (16) are found present in (19). The additional terms are interpreted as the electrical noise due to the detection process. The force estimator (18) can then be rewritten as

$$\widehat{F}_{\rm ext} = \Xi_{\rm m}\left(V_{\rm fr} + V_{\rm se}\right) \tag{20}$$

where $\Xi_{\rm m} V_{\rm fr}$ is given by (16) while $\Xi_{\rm m} V_{\rm se}$ collects all the other terms appearing in (19). Because of the normalization (18), these terms can be identified as those which are proportional to $\Xi_{\rm m}$. Physically, they represent the sensing error. They involve amplifier current and voltage noise as well as Nyquist noise associated to the loss and detection electrical lines. Since the amplifier voltage noise is present in both contributions $\Xi_{\rm m} V_{\rm fr}$ and $\Xi_{\rm m} V_{\rm se}$, it follows that these two contributions are not independent sources of noise.

The sensor noise spectrum $\Sigma_{\rm FF}$, *i.e.* the noise associated with fluctuations of $(\widehat{F}_{\rm ext} - F_{\rm ext})$, is now expressed as

$$\Sigma_{\rm FF} = \sum_\alpha |\mu_\alpha|^2\,\sigma^{\rm in}_{\alpha\alpha}. \tag{21}$$

As a consequence of the preceding discussion, this added noise spectrum can be written

$$\begin{aligned}
\Sigma_{\mathrm{FF}} &= |\Xi_{\mathrm{m}}|^2 \left(\sigma_{V_{\mathrm{fr}}V_{\mathrm{fr}}} + \sigma_{V_{\mathrm{se}}V_{\mathrm{se}}} + \sigma_{V_{\mathrm{fr}}V_{\mathrm{se}}}\right),\\
\sigma_{V_{\mathrm{fr}}V_{\mathrm{fr}}} &= \frac{2H_{\mathrm{m}}k_{\mathrm{B}}\Theta_{\mathrm{m}}}{|\Xi_{\mathrm{m}}|^2} + \frac{8R_{\mathrm{a}}\varkappa_{\mathrm{t}}^2 k_{\mathrm{B}}\Theta_{\mathrm{a}}}{|\Xi_{\mathrm{m}}|^2},\\
\sigma_{V_{\mathrm{se}}V_{\mathrm{se}}} &= \frac{\Omega^2}{\omega_{\mathrm{t}}^2\varkappa_{\mathrm{t}}^2}\left(\frac{1}{2R_{\mathrm{l}}}k_{\mathrm{B}}\Theta_{\mathrm{l}} + \frac{R_{\mathrm{r}}}{8|Z_{\mathrm{f}}|^2}k_{\mathrm{B}}\Theta_{\mathrm{r}}\right.,\\
&\quad \left. + R_{\mathrm{a}}\left(\frac{1}{|Z_{\mathrm{f}}|^2} + \frac{1}{R_{\mathrm{a}}^2} + \left|\frac{1}{R_{\mathrm{l}}} + \frac{1}{Z_{\mathrm{t}}}\right|^2\right)k_{\mathrm{B}}\Theta_{\mathrm{a}}\right),\\
\sigma_{V_{\mathrm{fr}}V_{\mathrm{se}}} &= 4R_{\mathrm{a}}C_{\mathrm{f}}\frac{K - M\Omega^2}{|\Xi_{\mathrm{m}}|^2}k_{\mathrm{B}}\Theta_{\mathrm{a}}.
\end{aligned} \tag{22}$$

The first two terms correspond to the noise spectrum of the velocity, the terms proportional to the factor $|\Xi_{\mathrm{m}}|^2$ represent the noise added by electrical detection. Finally the last line describes the result of the interference between these two contributions.

5 The cold damped accelerometer

The cold damped accelerometer consists in the sensor studied in the preceding section and the feedback loop used to generate the voltages applied on the electrodes to control the mass motion.

The motion is measured through the sensor signal r_1^{out} previously described after a synchronous demodulation. The feedback force applied for controlling the motion of the mass is obtained through a low frequency amplifier. The set of equations describing the complete accelerometer is the same as in the previous section (13–15) except for the equation of the proof mass motion (14) which is now read as

$$\begin{aligned}
\Xi_{\mathrm{m}}V_{\mathrm{cd}} &= F_{\mathrm{ext}} - \varkappa_{\mathrm{t}}Z_{\mathrm{t}}I_{\mathrm{t1}}\\
&\quad - \sqrt{2\hbar\,|\Omega|\,H_{\mathrm{m}}}m^{\mathrm{in}} - G_{\mathrm{s}}r_1^{\mathrm{out}} + F_{\mathrm{s}}^{\mathrm{in}}.
\end{aligned} \tag{23}$$

V_{cd} now denotes the velocity of the proof mass in presence of the cold damping. The term $G_{\mathrm{s}}r_1^{\mathrm{out}}$ represents the feedback action on the mass with the whole gain of the servo loop denoted G_{s}. The impedance of the detection line r is assumed to be small $R_{\mathrm{r}} \ll |Z_{\mathrm{f}}|$ so that its contribution is negligible. It is therefore equivalent to add a feedback proportional to r^{out} or proportional to the output voltage of the amplifier U_{r}. $F_{\mathrm{s}}^{\mathrm{in}}$ are the force fluctuations due to the active and passive elements used to generate the servo control force.

The solution of these equations yields the velocity of the cold damped mass

$$\begin{aligned}
\left(\Xi_{\mathrm{m}} + \Xi_{\mathrm{me}}\right)V_{\mathrm{cd}} &= F_{\mathrm{ext}} + \sum_{\alpha}\lambda_\alpha\alpha^{\mathrm{in}} + \sum_{\beta}\lambda_\beta\beta^{\mathrm{in}},\\
\Xi_{\mathrm{me}} &= H_{\mathrm{me}} + \frac{\mathrm{i}K_{\mathrm{me}}}{\Omega} = -\sqrt{\frac{2\omega_{\mathrm{t}}}{\hbar R_{\mathrm{r}}}}\frac{2\varkappa_{\mathrm{t}}Z_{\mathrm{f}}}{\Omega}G_{\mathrm{s}}.
\end{aligned} \tag{24}$$

The servo loop produces an effective mechanical impedance Ξ_{me} written as the sum of a damping term H_{me} and a restoring force of stiffness K_{me}, both parameters being frequency dependent. In particular K_{me} can include the effect of an integrator term in the feedback corrector. This term ensures the motionlessness of the mass at very low frequencies to the benefit of the instrument accuracy. The noise terms $\lambda_\alpha\alpha^{\mathrm{in}}$ represent the fluctuations due to the input fields α^{in} as in the previous section. In addition, there are noise terms $\lambda_\beta\beta^{\mathrm{in}}$ added by the active and passive elements in the servo loop.

Let us consider now the actual instrument case where the effective mechanical impedance Ξ_{me} is much larger than the free mass impedance Ξ_{m}

$$\begin{aligned}
H_{\mathrm{me}} &\gg H_{\mathrm{m}},\\
K_{\mathrm{me}} &\gg \left|K - M\Omega^2\right|.
\end{aligned} \tag{25}$$

These conditions are fully compatible with the stability of the feedback as evaluated in the design and demonstrated with the real instruments [1–3]. In the equations of motion written previously, this case corresponds to the limit of an infinite loop gain

$$G_{\mathrm{s}} \to \infty. \tag{26}$$

Then, the noise terms $\lambda_\beta\beta^{\mathrm{in}}$ coming from the servo loop scale as $\sqrt{G_{\mathrm{s}}}$. Hence their effect on velocity scales as

$$\frac{\lambda_\beta}{G_{\mathrm{s}}} \propto \frac{1}{\sqrt{G_{\mathrm{s}}}} \to 0 \tag{27}$$

so that they may be forgotten in (24). This only means that, as well known, the dominant noise sources are those associated with the first amplification stage, here the terms $\lambda_\alpha\alpha^{\mathrm{in}}$.

The velocity (24) stabilized by the feedback loop is now read as

$$\begin{aligned}
V_{\mathrm{cd}} &= -\sqrt{\frac{\hbar R_{\mathrm{r}}}{2\omega_{\mathrm{t}}}}\frac{\Omega}{2\varkappa_{\mathrm{t}}Z_{\mathrm{f}}}\sum_{\alpha}\frac{\lambda_\alpha}{G_{\mathrm{s}}}\alpha^{\mathrm{in}},\\
\frac{\lambda_{\mathrm{m}}}{G_{\mathrm{s}}} &= 0,\\
\frac{\lambda_{\mathrm{l}_2}}{G_{\mathrm{s}}} &= -\frac{2\mathrm{i}Z_{\mathrm{f}}}{\sqrt{R_{\mathrm{l}}R_{\mathrm{r}}}}, \quad \frac{\lambda_{\mathrm{l}_1}}{G_{\mathrm{s}}} = 0,\\
\frac{\lambda_{\mathrm{r}_1}}{G_{\mathrm{s}}} &= -1, \quad \frac{\lambda_{\mathrm{r}_2}}{G_{\mathrm{s}}} = 0,\\
\frac{\lambda_{\mathrm{a}_1}}{G_{\mathrm{s}}} &= -\frac{\lambda_{\mathrm{b}_1}}{G_{\mathrm{s}}} = 2\sqrt{\frac{R_{\mathrm{a}}}{R_{\mathrm{r}}}},\\
\frac{\lambda_{\mathrm{b}_1}}{G_{\mathrm{s}}} &= -2\mathrm{i}Z_{\mathrm{f}}\sqrt{\frac{R_{\mathrm{a}}}{R_{\mathrm{r}}}}\left(\frac{1}{R_{\mathrm{a}}} - \frac{1}{R_{\mathrm{l}}} - \frac{1}{Z_{\mathrm{t}}}\right),\\
\frac{\lambda_{\mathrm{b}_2}}{G_{\mathrm{s}}} &= -2\mathrm{i}Z_{\mathrm{f}}\sqrt{\frac{R_{\mathrm{a}}}{R_{\mathrm{r}}}}\left(\frac{1}{R_{\mathrm{a}}} + \frac{1}{R_{\mathrm{l}}} + \frac{1}{Z_{\mathrm{t}}}\right).
\end{aligned} \tag{28}$$

Since the servo loop efficiently maintains the mass at its equilibrium position, the velocity is no longer affected by the external force F_{ext}. However the sensitivity to external

force is still present in the correction signal which will be discussed later on. The residual motion of the mass is described by the various noise terms $\lambda_\alpha \alpha^{\rm in}/G_{\rm s}$. The values of these coefficients are easily interpreted through a comparison with the force estimator (18) evaluated in the preceding section for the capacitive sensor. The cold damped motion of the proof mass is indeed described by the simple equation

$$V_{\rm cd} = -V_{\rm se} \tag{29}$$

where $V_{\rm se}$ is the difference between the real velocity of the mass and the velocity measured by the sensor. This means that the servo loop efficiently corrects the motion of the mass except for the sensing error $V_{\rm se}$.

With the same set of equations (13–15) with (23 replacing 14), the output field $r_1^{\rm out}$ is evaluated and exploited as a measurement of the external force. As in the previous section, this output field is normalized so that the force estimator $\widehat{F}_{\rm ext}$ appears as the sum of the real force and of an equivalent force noise

$$\begin{aligned}\widehat{F}_{\rm ext} &= \sqrt{\frac{\hbar R_{\rm r}}{2\omega_{\rm t}}}\frac{\Omega \Xi_{\rm me}}{2\varkappa_{\rm t} Z_{\rm f}} r_1^{\rm out} \\ &= F_{\rm ext} + \sum_\alpha \mu_\alpha \alpha^{\rm in}.\end{aligned} \tag{30}$$

This expression is similar to the estimator (18) evaluated for the free mass although the free impedance $\Xi_{\rm m}$ has been replaced by the effective impedance $\Xi_{\rm me}$.

A quite remarkable result is then obtained. In the limit of the infinite loop gain and with the same approximations as above, the expressions of the coefficients μ_α are exactly the same as those (19) corresponding to the open loop case. The expression of the force estimator $\widehat{F}_{\rm ext}$ is the same as in the free case while the expression of the velocity is quite different. The actual motion of the mass is indeed independent of the external perturbations in the servo control case with the velocity determined by the sensor noise (29).

It is in fact possible to reexpress the force estimator (30) as the sum of two terms

$$\widehat{F}_{\rm ext} = \Xi_{\rm m}\left(V_{\rm fr} + V_{\rm se}\right) = \Xi_{\rm m}\left(V_{\rm fr} - V_{\rm cd}\right). \tag{31}$$

The first term is exactly the same as the actual motion (16) of the free running mass. It is the sum of the external force $F_{\rm ext}$ and of the force fluctuations exerted on the mass in the absence of servo control, namely the mechanical Langevin force and the back action force due to the sensor. The second term is the actual velocity (29) of the mass that is also the already discussed sensor error. Once again, these two terms are correlated since both depend on the same amplifier voltage noise. The expression of the noise spectrum $\Sigma_{\rm FF}$ is not reproduced here since it is exactly the same (22) as in the open loop case.

6 Discussion

The results obtained in the two previous sections allow to evaluate the performance of the cold damping technique for a wide range of experimental parameters and for all temperatures. In this concluding section, we want to discuss these results by focussing our attention on the present state-of-the-art instrument as well as on ultimate sensitivity limits which can be reached in the future with such an accelerometer.

The noise spectrum for the velocity of the proof mass in its free running regime may be rewritten

$$H_{\rm m}\sigma_{V_{\rm fr}V_{\rm fr}} = \frac{2}{1+\Delta^2}\left(k_{\rm B}\Theta_{\rm m} + 4\frac{R_{\rm a}}{R_{\rm m}}k_{\rm B}\Theta_{\rm a}\right). \tag{32}$$

The parameter Δ measures the reactive impedance of the free mass as compared to the dissipative one

$$\frac{K}{\Omega} - M\Omega = H_{\rm m}\Delta. \tag{33}$$

The electrical resistance $R_{\rm m}$ allows to express the mechanical damping coefficient $H_{\rm m}$ through the conversion relation

$$R_{\rm m} = \frac{H_{\rm m}}{\varkappa_{\rm t}^2}\,. \tag{34}$$

With this definition, the ratio $R_{\rm a}/R_{\rm m}$ allows to compare the electrical and mechanical noises in (32).

The noise spectrum $\sigma_{V_{\rm se}V_{\rm se}}$ for the sensing error $V_{\rm se}$, which is also the noise $\sigma_{V_{\rm cd}V_{\rm cd}}$ for the velocity $V_{\rm cd}$ of the proof mass in the cold damped regime, is expressed in a similar form

$$\begin{aligned}H_{\rm m}\sigma_{V_{\rm se}V_{\rm se}} = \frac{\Omega^2}{\omega_{\rm t}^2}\Bigg(&\frac{R_{\rm m}}{R_{\rm l}}k_{\rm B}\Theta_{\rm l} + \frac{R_{\rm m}R_{\rm r}}{4\left|Z_{\rm f}\right|^2}k_{\rm B}\Theta_{\rm r} \\ &+2R_{\rm a}R_{\rm m}k_{\rm B}\Theta_{\rm a}\left(\frac{1}{\left|Z_{\rm f}\right|^2} + \frac{1}{R_{\rm a}^2} + \left|\frac{1}{R_{\rm l}} + \frac{1}{Z_{\rm t}}\right|^2\right)\Bigg).\end{aligned} \tag{35}$$

The sensing error is minimized by diminishing the fluctuations coming from the electrical noise lines, that is when the transducer impedance $Z_{\rm t}$, the feedback impedance $Z_{\rm f}$ and the loss impedance $R_{\rm l}$ are chosen high enough. The transposition ratio $\Omega^2/\omega_{\rm t}^2$ appears as a common factor which greatly helps in keeping this error low.

The two contributions (32, 35) are added in the whole added noise spectrum $\Sigma_{\rm FF}$ together with a third term $\sigma_{V_{\rm fr}V_{\rm cd}}$

$$H_{\rm m}\sigma_{V_{\rm fr}V_{\rm se}} = 4\frac{R_{\rm a}}{\left|Z_{\rm f}\right|}\frac{\Omega}{\omega_{\rm t}}\frac{\Delta}{1+\Delta^2}k_{\rm B}\Theta_{\rm a}. \tag{36}$$

This term is also reduced when the feedback impedance $Z_{\rm f}$ is large.

Let us evaluate the whole noise spectrum $\Sigma_{\rm FF}$ for the specific case of the instrument proposed for the μSCOPE space mission devoted to the test of the equivalence

principle. The parameters have the following values

$$\begin{aligned} M &= 0.27 \text{ kg}, & H_\mathrm{m} &= 1.3 \times 10^{-5} \text{ kg s}^{-1}, \\ K &= 4 \times 10^{-6} \text{ N m}^{-1}, & \Delta &\simeq 100, \\ \frac{\Omega}{2\pi} &\simeq 5 \times 10^{-4} \text{ Hz}, & \frac{\omega_\mathrm{t}}{2\pi} &\simeq 10^5 \text{ Hz}, \\ \varkappa_\mathrm{t} &= 10^{-7} \text{ C m}^{-1}, & R_\mathrm{l} &= 2.5 \times 10^5 \ \Omega, \\ R_\mathrm{m} &= 1.3 \times 10^9 \ \Omega, & \Theta_\mathrm{m} &= 300 \text{ K}, \\ |Z_\mathrm{f}| &= 1.6 \times 10^5 \ \Omega, & |Z_\mathrm{t}| &= 10^{14} \ \Omega, \\ R_\mathrm{a} &= 0.15 \times 10^6 \ \Omega, & \Theta_\mathrm{a} &= 1.5 \text{ K}. \end{aligned} \tag{37}$$

In these conditions, the added noise spectrum is dominated by the mechanical Langevin forces

$$\begin{aligned} \Sigma_\mathrm{FF} &= 2H_\mathrm{m} k_\mathrm{B} \Theta_\mathrm{m} \\ &= 1.1 \times 10^{-25} \left(\text{kg m s}^{-2}\right)^2 / \text{Hz}. \end{aligned} \tag{38}$$

This corresponds to a sensitivity in acceleration

$$\frac{\sqrt{\Sigma_\mathrm{FF}}}{M} = 1.2 \times 10^{-12} \text{m s}^{-2} / \sqrt{\text{Hz}}. \tag{39}$$

Taking into account the integration time of the experiment, this is consistent with the expected instrument performance corresponding to a test accuracy of 10^{-15}.

In the present state-of-the-art instrument, the sensitivity is thus limited by the residual mechanical Langevin forces. The latter are due to the damping processes in the gold wire used to keep the proof mass at zero voltage [3]. With such a configuration, the detection noise is not a limiting factor. This is a remarkable result in a situation where the effective damping induced through the servo loop is much more efficient than the passive mechanical damping. This confirms the considerable interest of the cold damping technique for high sensitivity measurement devices.

Future fundamental physics missions in space will require even better sensitivities. To this aim, the wire will be removed and the charge of the test mass will be controlled by other means, for example UV photoemission. The mechanical Langevin noise will no longer be a limitation so that the analysis of the ultimate detection noise will become crucial for the optimization of the instrument performance. This also means that the electromechanical design configuration will have to be reoptimized taking into account the various noise sources associated with detection.

In order to evaluate these added noise sources we consider the whole noise spectrum obtained by taking into account the spectra (32, 35, 36)

$$\Sigma_\mathrm{FF} = H_\mathrm{m} \left(1 + \Delta^2\right) \left(\sigma_{V_\mathrm{fr} V_\mathrm{fr}} + \sigma_{V_\mathrm{se} V_\mathrm{se}} + \sigma_{V_\mathrm{fr} V_\mathrm{se}}\right). \tag{40}$$

This spectrum contains terms scaling as R_m as well as terms scaling as $1/R_\mathrm{m}$. Hence, there exists an optimum value for R_m when the other parameters as fixed. In the same way, it includes terms scaling as R_a and as $1/R_\mathrm{a}$ so that there exists an optimum value for R_a. In contrast, the noise is always lowered by reducing the electrical losses with large values for the impedances Z_t, Z_f and R_l and low values for R_r.

In these limits, the added noise spectrum Σ_FF takes a simple form

$$\begin{aligned} \Sigma_\mathrm{FF} = 2H_\mathrm{m} k_\mathrm{B} \Theta_\mathrm{m} + 8H_\mathrm{m} \frac{R_\mathrm{a}}{R_\mathrm{m}} k_\mathrm{B} \Theta_\mathrm{a} \\ + 2H_\mathrm{m} \left(1 + \Delta^2\right) \frac{\Omega^2}{\omega_t^2} \frac{R_\mathrm{m}}{R_\mathrm{a}} k_\mathrm{B} \Theta_\mathrm{a}. \end{aligned} \tag{41}$$

This final result is optimized by matching the values of the impedances R_a and R_m so that

$$\begin{aligned} \left(\frac{R_\mathrm{a}}{R_\mathrm{m}}\right)^\mathrm{opt} &= \frac{\sqrt{1+\Delta^2}}{2} \frac{|\Omega|}{\omega_\mathrm{t}}, \\ \Sigma_\mathrm{FF}^\mathrm{opt} &= 2H_\mathrm{m} k_\mathrm{B} \Theta_\mathrm{m} + 8H_\mathrm{m} \sqrt{1+\Delta^2} \frac{|\Omega|}{\omega_\mathrm{t}} k_\mathrm{B} \Theta_\mathrm{a}. \end{aligned} \tag{42}$$

This is the sum of the already discussed limit associated with mechanical Langevin fluctuations and of a second term which represents the ultimate detection noise. The first contribution dominates the second one for the present state-of-the-art instrument but this will no longer be the case for future instruments designed for better performance tests of the equivalence principle. For such instruments, equation (42) shows that the sensitivity may be largely improved.

Thanks are due to Alain Bernard, Vincent Josselin and Eric Willemenot for helpful discussions.

References

1. A. Bernard, P. Touboul, The GRADIO accelerometer: design and development status, *Proc. ESA-NASA Workshop on the Solid Earth Mission ARISTOTELES*, Anacapri, Italy, 1991.
2. P. Touboul *et al.*, Continuation of the GRADIO accelerometer predevelopment, ONERA Final Report 51/6114PY, 62/6114PY ESTEC Contract (1992, 1993).
3. E. Willemenot, Ph.D. thesis, University Paris-Sud, 1997.
4. J.M.W. Milatz, J.J. van Zolingen, Physica **XIX**, 181 (1953); J.M.W. Milatz, J.J. van Zolingen, B.B. van Iperen, Physica **XIX**, 195 (1953).
5. A. Maraner, S. Vitale, J.P. Zendri, Class. Quantum Gravity **13**, A129 (1996).
6. D.B. Newell *et al.*, Rev. Sci. Instr. **68**, 3211 (1997); S.J. Richman *et al.*, Rev. Sci. Instr. **69**, 2531 (1998).
7. D.G. Blair *et al.*, Phys. Rev. Lett. **74**, 1908 (1995).
8. A. Einstein, Ann. Physik **17**, 549 (1905).
9. H. Nyquist, Phys. Rev. **32**, 110 (1928).
10. R. Kubo, Rep. Prog. Phys. **29**, 255 (1966).
11. E.M. Lifshitz, L.P. Pitaevskii, *Landau and Lifshitz, Course of Theoretical Physics, Statistical Physics Part 2* (Butterworth-Heinemann, 1980), Chap. VIII.
12. H.B. Callen, T.A. Welton, Phys. Rev. **83**, 34 (1951).

13. Y. Yamamoto, S. Machida, S. Saito, N. Imoto, T. Yanagawa, N. Kitagawa, G. Björk, *Progress in Optics XXVIII*, edited by E. Wolf (Elsevier, 1990), p. 87.
14. S. Reynaud, A. Heidmann, E. Giacobino, C. Fabre, *Progress in Optics XXX*, edited by E. Wolf (Elsevier, 1992), p. 1.
15. V.B. Braginsky, F.Ya. Khalili, *Quantum Measurement* (Cambridge University Press, 1992).
16. P. Grangier, J.M. Courty, S. Reynaud, Opt. Commun. **89**, 99 (1992).
17. P. Bonifazi, C. Cinquegrana, E. Majorana, N. Pergola, P. Puppo, P. Rapagnani, F. Ricci, S. Vaselli, M. Visco, Phys. Lett. A **215**, 141 (1996).
18. M.F. Bocko, R. Onofrio, Rev. Mod. Phys. **68**, 755 (19696).
19. H. Heffner, Proc. IRE **50**, 1604 (1962).
20. H.A. Haus, J.A. Mullen, Phys. Rev. **128**, 2407 (1962).
21. J.P. Gordon, L.R. Walker, W.H. Louisell, Phys. Rev. **130**, 806 (1963).
22. C.M. Caves, Phys. Rev. D **26**, 1817 (1982).
23. R. Loudon, T.J. Shephered, Optica Acta **31**, 1243 (1984).
24. Y. Yamamoto, N. Imoto, S. Machida, Phys. Rev. A **33**, 3243 (1986).
25. A. Liebman, G.J. Milburn, Phys. Rev. A **33**, 634 (1993).
26. J. Meixner, J. Math. Phys. **4**, 154 (1963).
27. B. Yurke, J.S. Denker, Phys. Rev. A **29**, 1419 (1984).
28. C.W. Gardiner, IBM J. Res. Dev. **32**, 127 (1988).
29. J.-M. Courty, S. Reynaud, Phys. Rev. A **46**, 2766 (1992).
30. F. Grassia, Ph.D. thesis, University P. & M. Curie, 1998.
31. J.-M. Courty, F. Grassia, S. Reynaud, Europhys. Lett. **46**, 31 (1999).